EXPERIMENTAL METHODS

Electrolytes and electrodes

NCM811 powder, poly (vinyl difluoride) (PVDF) and Super P were mixed in N-methyl pyrrolidone (NMP) at a weight ratio of 8:1:1, stirred for a few hours and evenly coated on aluminium foil, then baked in a vacuum oven at 80℃ for 12 h. The laminate was cut into discs (diameter 12 mm). Areal mass loading of NCM811 on discs was ~1.5 mg cm^{-2}. 1.0M Lithium Hexafluorophosphate ($LiPF_6$) in Ethylene carbonate (EC): Ethyl Methyl Carbonate (EMC)=3:7 Vol% (v/v = 1/1) without other additives was applied as the base electrolyte, added a certain amount of MTC to base electrolyte to form modified electrolyte. Polypropylene (PP) was applied as the separator.

Electrochemical tests

Symmetric cells (both Li-Li foils were applied as working and counter electrodes), the Li||Cu cells and Li||NCM811 cells were assembled as CR2032 or CR2025 coin cells in a glove box filled argon (both H_2O and O_2 concentrations below 0.1 ppm), the amount of electrolyte added to each cell is controlled at 40-50μL. All cell tests were carried out on NEWARE battery testers inside temperature chambers with the temperature held at 25 ℃ or 50 ℃. The voltage windows for Li||NCM811 cells cycling were 2.5-4.3 V or 2.5-4.6 V. Li plating/stripping measurements were performed on NEWARE multichannel battery testing system at 25 ℃. EIS (Electrochemical Impedance Spectroscopy) tests were carried out on the CHI660D electrochemical workstation in the frequency range of 0.1-10^6 Hz. NCM811 was used as cathode material for Li||NCM811 cells (CR2025). The Li||NCM811 cells were tested in a

voltage range of 2.8-4.3 V on NEWARE multichannel battery testing system.

Characterizations

The method for measuring hydrofluoric acid is described as follows: weigh about 20 g of electrolyte (accurate to 0.01 g) and quickly pour it into a beaker containing 100 mL of the ice-water mixture without stopping stirring. Add 10 drops of bromothymol blue (0.1% ethanol solution) as an indicator and titrate quickly with NaOH solution until the solution turns blue.

The morphology of the electrodes was examined by a field emission scanning electron microscope (SU8010, Hitachi) equipped with an energy dispersive X-ray spectroscopy detector (INCA Energy, Oxford Instruments). X-ray diffraction (XRD, Panalytical Aries) was performed to investigate the crystal structure of the electrode materials after cycling with 2θ intervals between 10° and 90° through Cu Kα 1.54059 Å. In addition, the surface film characterization was analyzed by X-ray photoelectron spectroscopy (XPS, PHI VersaProbe 4). The binding energy was corrected based on the C 1s peak of hydrocarbon at 284.8 eV. Prior to measurements, the cells are disassembled in an argon-filled glove box to retrieve electrode samples. And all the samples were rinsed with an ethylene carbonate (EC) solvent to remove the residual electrolyte salt and by-products.
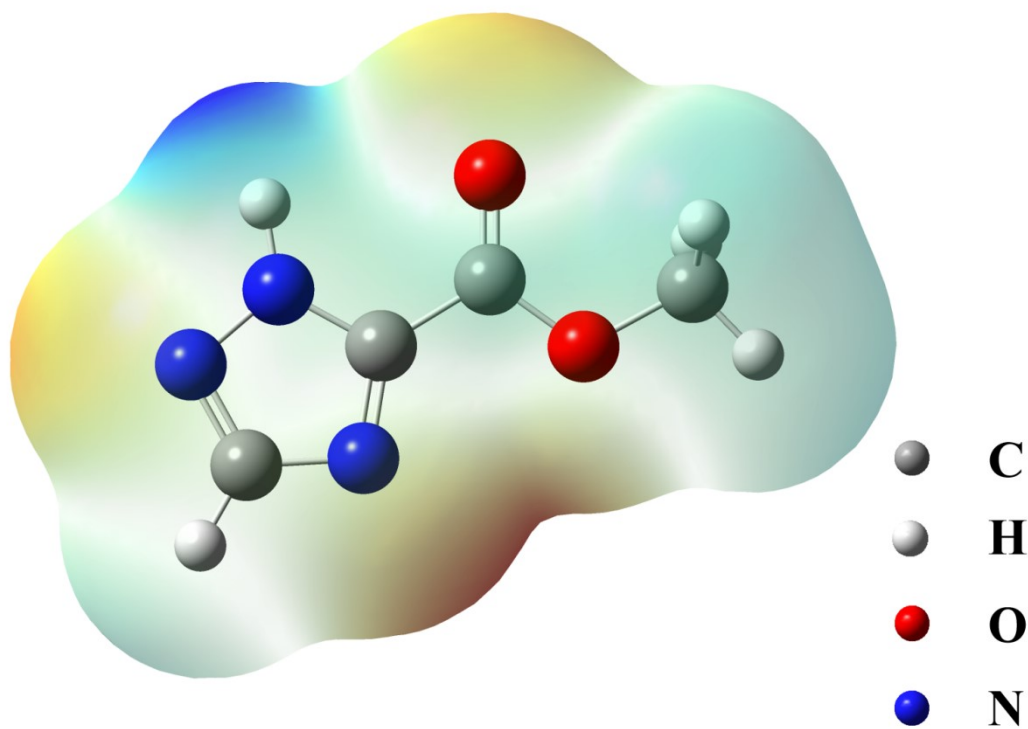
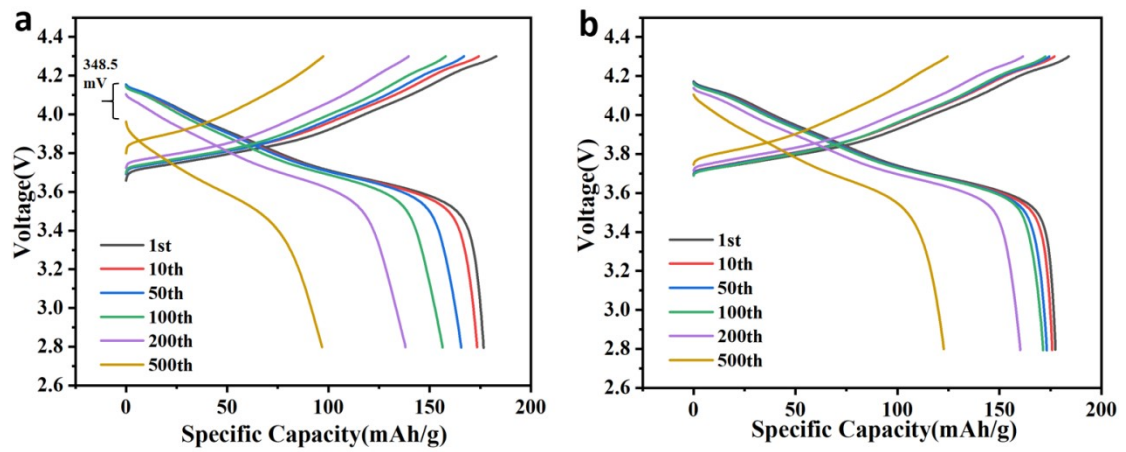**Figure S1**. The electrostatic potential of MTC molecule.

Figure S2. The long cycling voltage-specific capacity curves of the cells without and with MTC. (a) Without MTC; (b) With MTC.

After 500 cycles, the overpotential of the cell with MTC was only 53.6 mV, while the overpotential of the cell without MTC was higher, specifically 319.3 mV, which was also a reason for the rapid attenuation of the capacity without MTC.
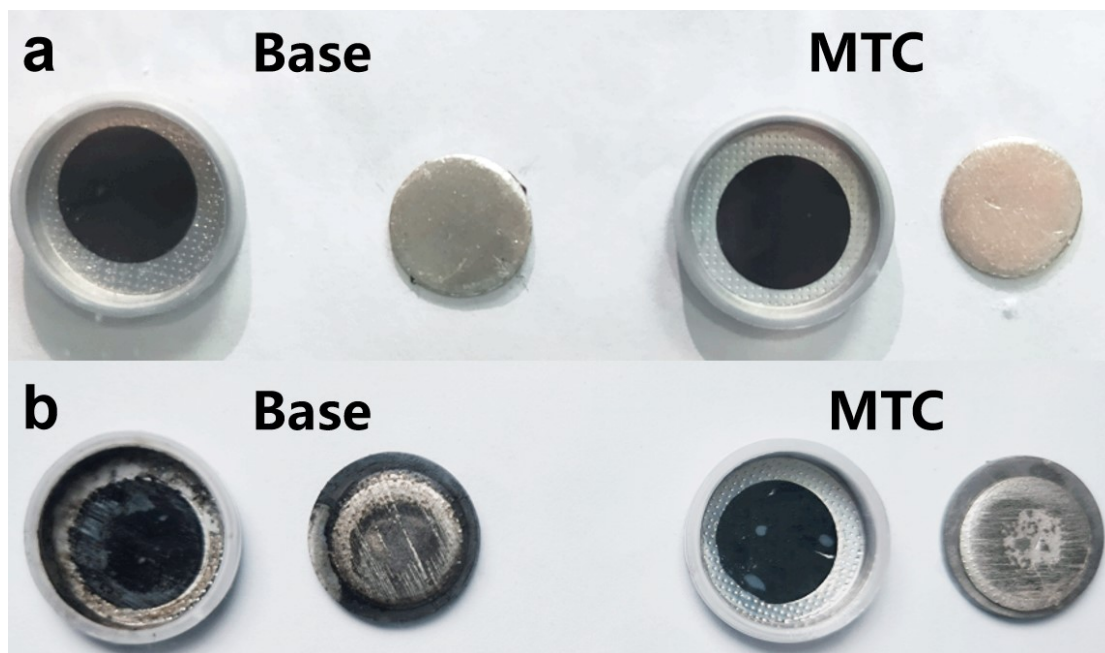
Figure S3. Optical images of anode, cathode and separator. (a) Cells before long cycling test.

(b) Cells after long cycling test.

Fig. S3 shows the interior of the Li||NCM811 cells after a long cycle test. Many

black materials were identified on the anode and separator in the cell without MTC.
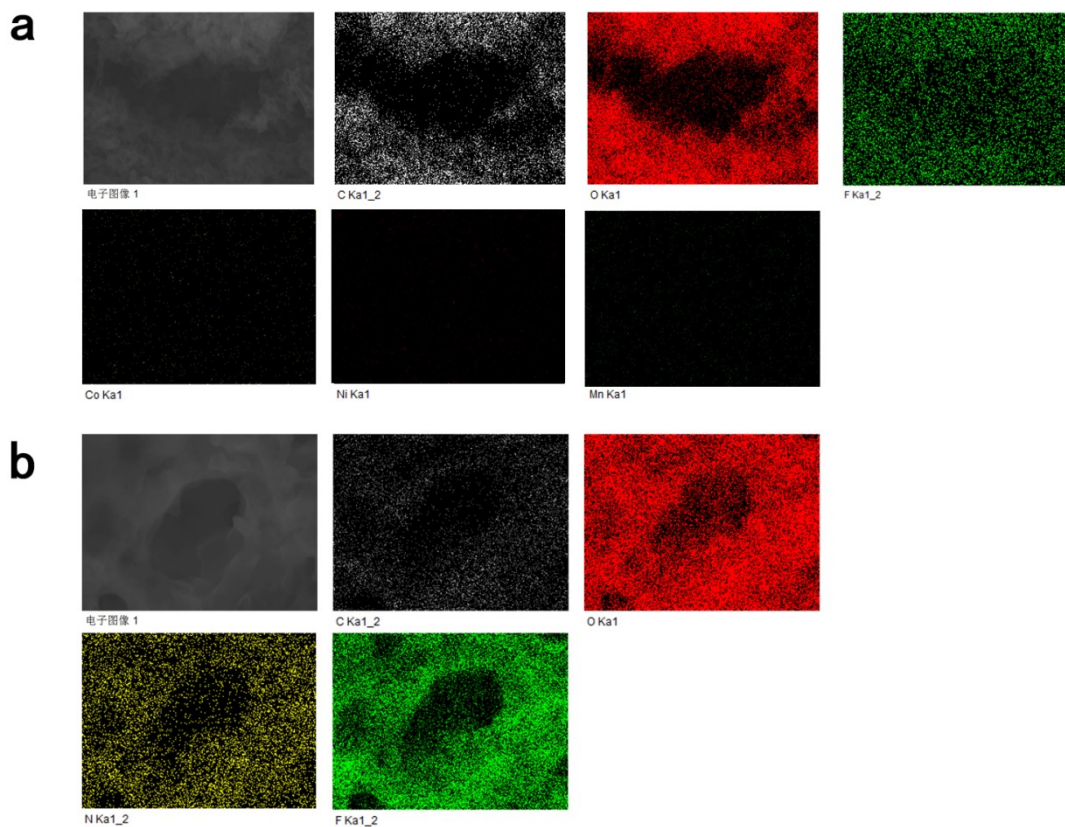
Figure S4. EDS images of Li anode surface after long cycle test. (a) Without MTC; (b) With MTC.

The absence of transition metal elements detected at the anode in the energy dispersive spectroscopy (EDS) test ruled out the hypothesis that the black material was formed by dissolved transition metal element. Therefore, the black substance was confirmed to be dead lithium and products of side reactions formed by the anode.
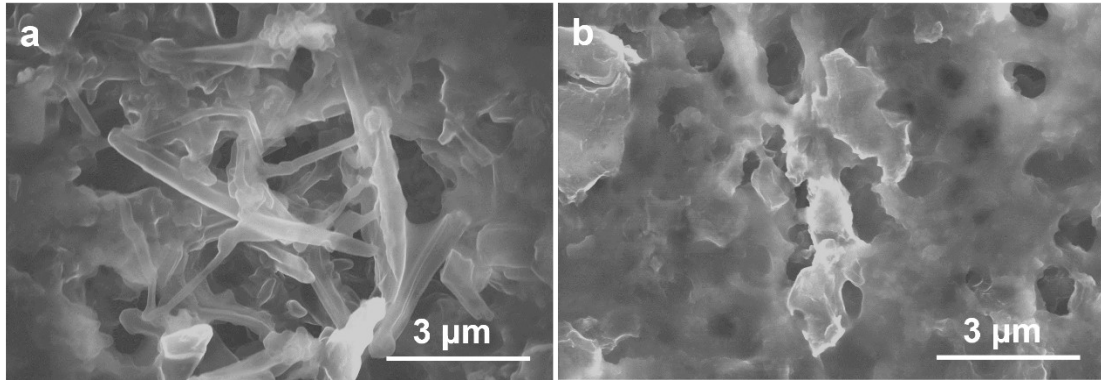
Figure S5. SEM images of Li anode surface after long cycle test. (a) Without MTC; (b) With MTC.
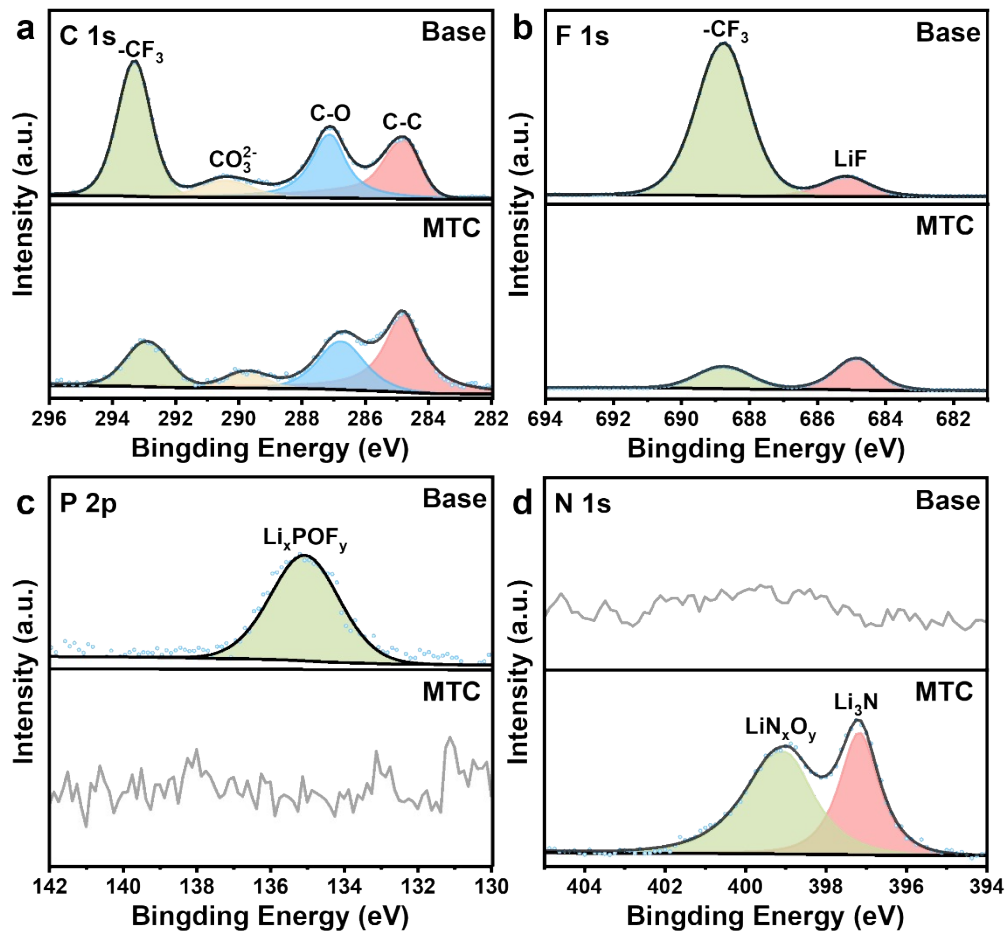
Figure S6. Surface film characterization of lithium anode. (a) C 1s. (b) F 1s. (c) P 2p. (b) N 1s XPS spectra with and without and with MTC.

In the C 1s spectrum, the peak at 292.9 eV corresponds to -CF$_3$, and the peaks at 289.9 eV, 286.8 eV and 284.8 eV were originated from the species of -CO$_3^{2-}$, C-O and C-C/C-H species respectively. The peak at 289.9 eV corresponds to the insoluble electrolyte reduction product produced by solvent decomposition, and the bond peak at 292.9 eV corresponds to the decomposition of LiFP$_6$ conductive salt in the electrolyte.[1,2] The existence of MTC not only reduces the reduction of solvents, but also greatly inhibits the occurrence of decomposition as a side reaction. In the F 1s spectrum, the peaks at 688.8 eV and 684.9 eV represent the presence of -CF$_3$ and LiF, as mentioned above, the appearance of F-containing species represents the

decomposition of $LiPF_6$ in the electrolyte, the decomposition peak of $LiPF_6$ also can find at 135.1 eV in P 2p spectra. Obviously, the cells with MTC had less $LiPF_6$ decomposition and a higher proportion of LiF was formed, which helps to form the SEI layer rich in LiF. LiF has a higher elastic modulus, making lithium deposition more compact and orderly in the anode. Moreover, the high ionic conductivity of LiF-rich SEI can reduce the diffusion barrier of Li^+ on the surface and then prevent the transmission of electrons.[3,4] In N 1s spectra, the peaks at 397.1 eV and 399.0 eV are attributed to Li_3N and LiN_xO_y, it is found that MTC will decompose to substances with rapid Li^+ transfer ability in anode.[5] Less decomposition of $LiPF_6$ and SEI composed with a higher portion of LiF make the anode have more stable properties.
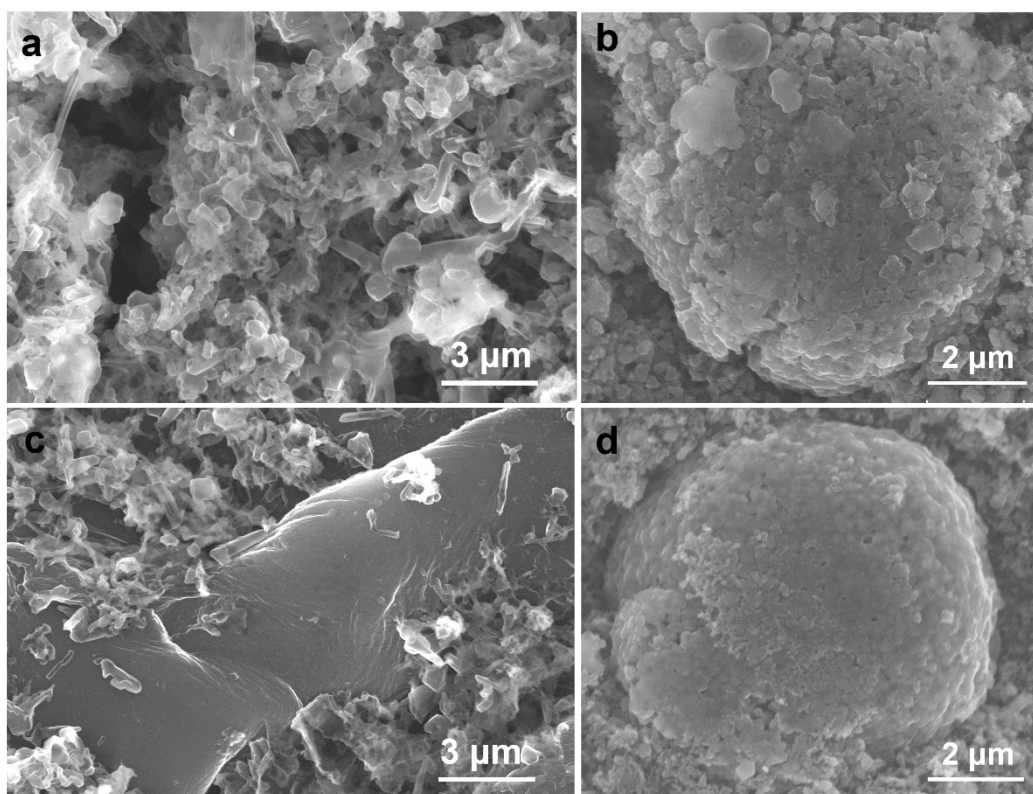
Figure S7. SEM images after reverse buckle test of the electrodes. The SEM image of (a) Li anode and (b) NCM811 cathode without MTC; The SEM image of (c) Li anode and (d) NCM811 cathode with MTC.

The surface of the anode without MTC contained many lithium dendrites (Fig. S7a, ESI†). The anode of the cell with MTC is shown in Fig. S7c (ESI†). The bottom layer of the anode surface was observed to be smooth and orderly, corresponding to the results of the C-rate test when adding MTC. And lithium dendrites were observed in the top layer, corresponding to the cycling test results for the electrolyte without MTC. NCM811 cathode particles showed cracks and in some cases even a structural collapse (Fig. S7b, ESI†). With MTC, as shown in Fig. S7d (ESI†), the structure of the NCM811 particles was basically intact.
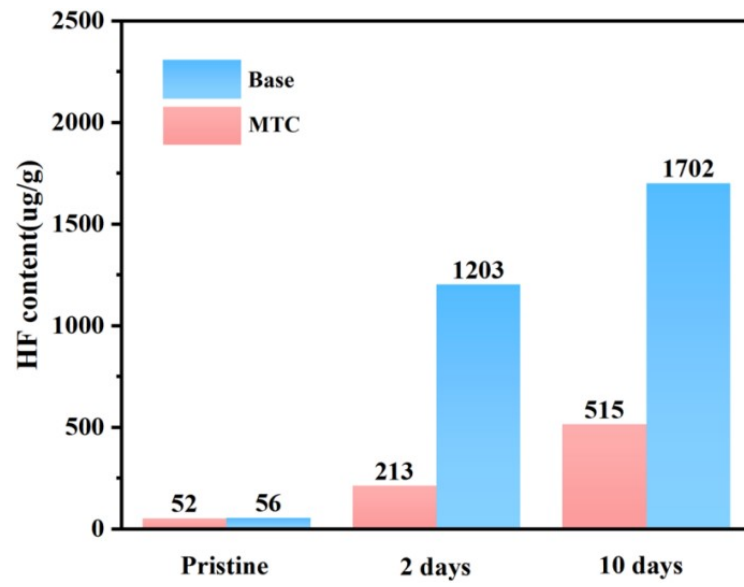
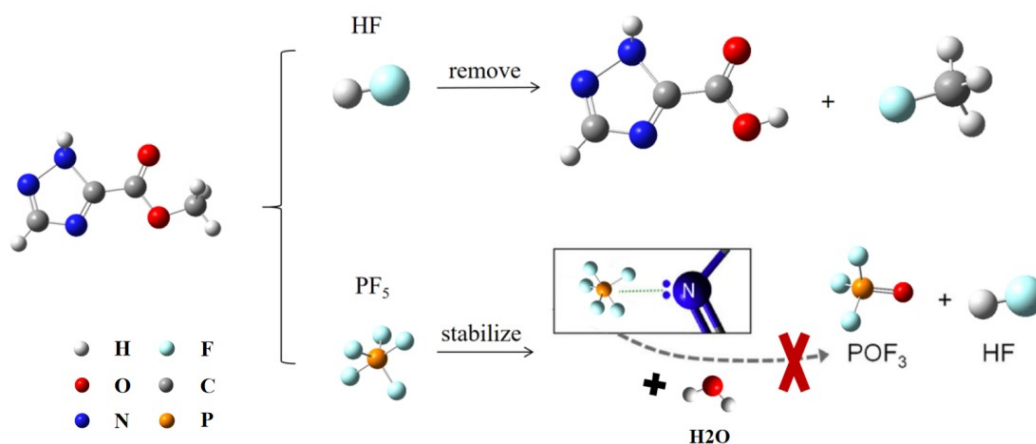**Figure S8.** HF content of electrolytes under different conditions.

Figure S9. Schematic diagram of the mechanism of MTC stabilizing electrolyte at high temperature.

It can be seen from Equations 1, 2 and Figure S9 that there is a linear relationship between the content of HF and POF_3.[6] At present, the testing method of HF content is more advanced and the result is more accurate, and HF is the primary cause of electrolyte deterioration. Therefore, this paper considers that only testing the content of HF can completely show the inhibition function of MTC on electrolyte deterioration.
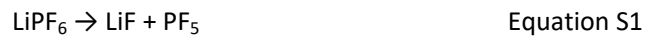
$$CE_{avg} = \frac{nQ_C + Q_S}{nQ_C + Q_T}$$

Formula

S1

where Q_S stands for dissolution capacity; Q_T stands for deposition capacity; Q_C stands for cyclic capacity; n stands for the number of cycles

$$t_{Li}^+ = \frac{I_S(V - R_0 I_0)}{I_0(V - R_S I_S)}$$

Formula S2

Where I_S stands for current of the cell after test; I_0 stands for current of the cell before the test; R_S stands for impendence of the cell after test; R_0 stands for impendence of the cell before the test.

$$LiPF_6 \rightarrow LiF + PF_5$$

Equation S1

$$PF_5 + H_2O \rightarrow POF_3 + 2HF$$

Equation S2

References

(1) Chang. S, Jin. X, He. Q, Liu. T, Fang. J, Shen. Z, Li. Z, Zhang. S, Dahbi. M, Alami. J, Amine. K, Li. A, Zhang. H and Lu. J, *Nano Lett.,* 2022, **22**, 263-270.

(2) Cao. W, Chen. W, Lu. M, Zhang. C, Tian. D, Wang. L and Yu. F, *J. Energy Chem.,* 2023, **76**, 648-656.

(3) Mu. T, Sun. Y, Wang. C, Zhao. Y, Doyle-Davis. K, Liang. J, Sui. X, Li. R, Du. C, Zuo. P, Yin. G and Sun. X, *Nano Energy,* 2022, **103**, 107829.

(4) Li. X, Liu. J, He. J, Qi. S, Wu. M, Wang. H. Jiang. G, Huang. J, Wu. D, Li. F and Ma. J, *Adv. Sci.,* 2022, **9**, 2201297.

(5) Wang. X, Li. S, Zhang. W, Wang. D, Shen. Z, Zheng. J, Zhuang. H, He. Y and Lu. Y., *Nano Energy,* 2021, **89**, 106353.

(6) Aravindan. V, Gnanaraj. J, Madhavi. S and Liu. H, *Chemistry-a European Journal*, 2011, **17**, 14326-14346.